IEEE Access
Multidisciplinary | Rapid Review | Open Access Journal

Received July 31, 2018, accepted August 30, 2018, date of publication September 10, 2018, date of current version October 12, 2018.

Digital Object Identifier 10.1109/ACCESS.2018.2869529

Artificial-Noise-Aided Secure Transmission for Proximal Legitimate User and Eavesdropper Based on Frequency Diverse Arrays

BIN QIU[1,2], JIAN XIE[1,2], LING WANG[1,2], AND YUEXIAN WANG[2,3]

[1]Research and Development Institute of Northwestern Polytechnical University in Shenzhen, Shenzhen, 518057, China
[2]School of Electronics and Information, Northwestern Polytechnical University, Xi'an 710072, China
[3]School of Electrical and Electronic Engineering, The University of Adelaide, Adelaide, SA 5005, Australias

Corresponding authors: Jian Xie (xiejian@nwpu.edu.cn) and Ling Wang (lingwang@nwpu.edu.cn)

This work was supported in part by the National Key Research and Development Program of China under Grant 2018YFB0505104, in part by the Shenzhen Science and Technology Innovation Committee of Basic Research Projects under Grant JCYJ20170306154016149 and Grant JCYJ20170815154325384, in part by the National Natural Science Foundation of China under Grant 61601372, in part by the China Postdoctoral Science Foundation under Grant 2017M613200, in part by the Natural Science Basic Research Plan in Shaanxi Province of China under Grant 2017JQ6068, and in part by the Shanghai Aerospace Science and Technology Innovation Fund under Grant sast2017-077.

ABSTRACT In this paper, we aim to address the physical layer security problem for proximal legitimate user (LU) and eavesdropper (Eve) in the case of close-located LU and Eve, where conventional directional modulation (DM) methods may fail to provide efficient secure performance. In order to handle this problem, an optimal frequency offsets of frequency diverse array-based DM with artificial noise (AN) scheme is proposed. We maximize the secrecy capacity by optimizing the frequency offsets and designing AN projection matrix. The optimization problem of the frequency offsets is solved by a block successive upper-bound minimization method to iteratively obtain stationary convergence solutions. By elaborately calculating frequency offsets across array antennas, we can decouple the angle-range correlation and maximize recreational secrecy capacity, resulting in the improvement of the security performance of wireless communications. Numerical results show that the proposed method can provide a higher secrecy capacity than conventional DM schemes with the changes of bandwidth, power allocation factor, and power for the case of proximal LU and Eve. In addition, the proposed scheme is suitable for the case of multi-Eves.

INDEX TERMS Directional modulation (DM), frequency diverse array (FDA), physical layer security, artificial noise (AN).

I. INTRODUCTION

Wireless communications allow information flow through broadcasting. However, eavesdropper may also receive the information. New researches on physical layer security primarily focus on guaranteeing communication signals with low probability of interception (LPI) and low probability of detection (LPD) [1], [2]. In order to achieve security of free space wireless communications with LPI or/and LPD, frequency diversity arrays directional modulation technology (FDA-DM) [3]–[7] is a potential way due to FDA-DM's distinct characteristic [8]–[11] that amplitude and spatial distribution of transmitted signals can be controlled by the frequency offsets, the number of array elements, and beamforming vector.

Recently, FDA-DM has been widely used in wireless communications. Xiong *et al.* [12], [13] employ genetic algorithm for optimizing the beamforming vector to achieve the physical layer security in both angle and range dimensions. To improve confidentiality, the work presented in [14]–[16] uses non-linearly increasing frequency offsets (square and cubic increasing, logarithmically increasing, and random frequency offsets) to decouple the correlation between the direction and range of FDA transmit beampattern. A structure named MIMO array antennas with beamforming on transmit is proposed in [17]–[20], which applies the frequency diversity to the phased-MIMO array. A weighted fractional Fourier transform using polarization modulation is proposed in [22]–[24], where the confidential message is concealed in the polarization state of the carrier.

Besides the above transmit beamforming on the radio frequency (RF) frontend, work in [25]–[27] focuses on the baseband technology to provide physical layer security.

In [28], a wireless secrecy transmission scheme is proposed to transmit confidential messages to the desired user securely and precisely by the joint use of multiple techniques, including artificial noise (AN) projection, phase alignment/beamforming, random subcarrier selection, and DM. In addition, researchers in [29]–[31] combine random frequency diverse arrays directional modulation with artificial-noise (R-FDA-DM-AN) to realize confidential transmission, which enables the transmitter to transmit AN, as an interference signal of eavesdropper (Eve), and useful messages together, such that the orthogonal projection matrix only interferes the Eve without affecting the legitimate user (LU). Therefore, implementing AN on baseband can make eavesdroppers hard to detect useful signals, and further improve security of wireless communications.

In practice, knowing the location of LU, the Eve can be located as close as possible to LU to wiretap confidential information. In the case of proximal LU and Eve, we suppose DM system consists of a transmitter with an N-element antenna array and one or many Eves with a single antenna located very close to the LU. The current study on aforementioned security schemes, however, either focuses on the design of the beamforming vector or the decoupled methods, cannot deal with the security for proximal LU and Eve, as it is hard for only using AN-aided secure transmission or FDA-DM to guarantee the performance of security. In [32], secure transmission based on R-FDA-DM-AN scheme was proposed. R-FDA-DM-AN has a good performance of decoupling, but it cannot guarantee the maximum secrecy capacity for the random frequency offsets. Lin *et al.* [33] optimize the frequency offsets of FDA to maximize the secrecy capacity, but the optimization requires a continuous update of the beamformer by calculating eigenvectors, and if the Eve is sensitive enough or the relative locations of Eve and LU have some robustness, the algorithm may suffer from severe security performance degradation since the minimum signal-to-noise ratio (SNR) of the Eve is limited without aided AN.

In this paper, we adopt the AN-aided secure transmission in the DM technique based on FDA to satisfy the security needs for proximal LU and Eve, i.e., leveraging AN and FDA-DM to further reduce the signal-to-artificial-noise ratio (SANR) of Eve and enhance the confidentiality. As discussed earlier that the frequency offsets in FDA among different array antennas play an important role in angle-range dependent energy transmission, we propose to maximize the secrecy capacity between the LU and Eve by optimizing the frequency offsets of FDA-DM-AN. Next, to calculate the stationary optimal frequency offsets, we use the block successive upper bound minimization (BSUM) algorithm [34]. Finally, we extend the approach to the case of multi-Eves.

The rest of this paper is organized as follows. In Section II, we detail our system model. Then, we analyze the secrecy capacity and provide an optimal solution of the problem in Section III. Section IV presents the multi-Eves system and extends our optimal method to this problem. The performance of the proposed scheme is numerically evaluated in Section V, and then Section VI draws conclusions.

Notations: Throughout this paper, we adopt the following notations. Matrices, vectors, and scalars are denoted by upper-case, lower-case bold-faced letters, and lower-case letters, respectively. The superscripts $(\cdot)^T$, $(\cdot)^*$ and $(\cdot)^H$ represent transpose, conjugate, and Hermitian operators, respectively. Denote $\|\cdot\|_2$ and $|\cdot|$ as the ℓ_2-norm and absolute value of a scalar, respectively. $\mathbb{E}[\cdot]$, $\mathrm{tr}(\cdot)$ and $\det(\cdot)$ indicate the expectation, trace, and determinant operators. The notations $\mathbb{R}$ and $\mathbb{C}$ represent to the real and complex number domains, respectively.

II. SYSTEM MODEL

A. FREQUENCY DIVERSE ARRAYS

In the DM system, as shown in Fig. 1(a), the transmitter is deployed with an N-element linear antenna array. The constant distance between the two elements is d . The FDA is different from the phased array (PA) for the frequency of each element is different. The radiated frequency at the mth element is f_m, $m = 0, 1...N-1$. Generally, set the first element as the reference. The steering vector of location (r, θ) at time instant t is given by [28]

$$\mathbf{h}(\mathbf{f}, \theta, r, t) \triangleq \big[h_0(f_0, \theta, r, t), ..., h_m(f_m, \theta, r, t), ..., h_{N-1}, (f_{N-1}, \theta, r, t)\big]^T \in \mathbb{C}^{N\times 1}, \quad (1)$$

where $h_m(f_m, \theta, r, t) \triangleq e^{-j2\pi f_m(t-\frac{r-md\sin\theta}{c})}$, $m = 0, 1, \ldots, N-1$, and c is the speed of light. Define the frequency offsets vector as $\mathbf{f} \triangleq [f_0, f_1, ..f_{N-1}]^T \in \mathbb{R}^{N\times 1}$. It is assumed that the locations of LU and Eve are known, and thus define (r_L, θ_L) and (r_E, θ_E) as the coordinates of the LU and Eve, respectively. We assume LU and Eve are very close, i.e., $(r_L, \theta_L) \approx (r_E, \theta_E)$. To simplify the expression, $\mathbf{h}_L(\mathbf{f}, t)$ and $\mathbf{h}_E(\mathbf{f}, t)$ are denoted as the steering vectors of LU and Eve at time t, respectively, i.e., $\mathbf{h}_L(\mathbf{f}, t) \triangleq \mathbf{h}(\mathbf{f}, \theta_L, r_L, t)$, $\mathbf{h}_E(\mathbf{f}, t) \triangleq \mathbf{h}(\mathbf{f}, \theta_E, r_E, t)$.

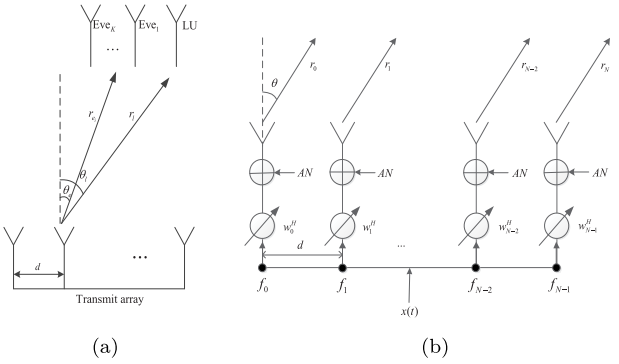

FIGURE 1. Model of FDA beamforming for (a) DM system, (b) Transmit AN-aided signal.

B. FREQUENCY DIVERSE ARRAY-BASED DIRECTIONAL MODULATION WITH ARTIFICIAL NOISE

FDA-DM-AN has been widely used in physical layer security of wireless communications due to its satisfactory secrecy performance [35]. AN is deliberately superimposed on the baseband transmit signal. The LU will not be affected by the AN since the column vectors of AN projection matrix lie in the null space of steering vector of the LU, whereas the SANR will be significantly reduced at Eve such that Eve cannot decipher the messages.

We first design the AN by calculating a projection matrix and then project the aided AN to the null space of conjugate transpose of the steering vector along LU. The AN vector $\mathbf{z}$ is independent and identically distributed (i.i.d) complex Gaussian random variables, i.e., $\mathbf{z} \sim \mathcal{CN}(0, \mathbf{I}_N)$. The residual vector is orthogonal to span($\mathbf{h}_L(\mathbf{f}, t)$) [36], i.e.,

$$\mathbf{h}_L^H(\mathbf{f}, t)(\mathbf{z} - \zeta \mathbf{h}_L(\mathbf{f}, t)) = 0. \tag{2}$$

Next, we obtain $\zeta = \frac{\mathbf{h}_L^H(\mathbf{f},t)\mathbf{z}}{\mathbf{h}_L^H(\mathbf{f},t)\mathbf{h}_L(\mathbf{f},t)}$. Substituting ζ into $\mathbf{z} - \zeta \mathbf{h}_L(\mathbf{f}, t)$, we obtain

$$\mathbf{z} - \zeta \mathbf{h}_L(\mathbf{f}, t) = (\mathbf{I}_N - \frac{\mathbf{h}_L(\mathbf{f}, t)\mathbf{h}_L^H(\mathbf{f}, t)}{N})\mathbf{z}. \tag{3}$$

The matrix $\mathbf{I}_N - \frac{\mathbf{h}_L(\mathbf{f},t)\mathbf{h}_L^H(\mathbf{f},t)}{N}$ can project $\mathbf{z}$ into the null space of conjugate transpose of the steering vector of LU. Therefore the projection matrix is given by

$$\mathbf{P}_{AN}(t) \triangleq \mathbf{I}_N - \frac{\mathbf{h}_L(\mathbf{f}, t)\mathbf{h}_L^H(\mathbf{f}, t)}{N}, \tag{4}$$

and thus the normalized AN can be expressed as

$$\mathbf{n}_{AN}(t) = \frac{\mathbf{P}_{AN}(t)\mathbf{z}}{\|\mathbf{P}_{AN}(t)\mathbf{z}\|_2}. \tag{5}$$

As shown in Fig. 1(b), the AN-aided signal transmitted at time instant t can be expressed as

$$\mathbf{s}(t) = \sqrt{\alpha P_s}\mathbf{w}(t)x(t) + \sqrt{(1-\alpha)P_s}\mathbf{n}_{AN}(t), \tag{6}$$

where P_s is the transmitting power, α is the power allocation factor between the useful signal and AN, and $x(t)$ is the symbol of complex transmitting confidential message with average power $\mathbb{E}\left[|x(t)|^2\right] = 1$. The beamforming vector at time t is $\mathbf{w}(t) \triangleq [w_0(t), w_1(t), ...w_{N-1}(t)]^T \in \mathbb{C}^{N\times 1}$. Based on the DM [31], the beamforming vector at time t is given by

$$\mathbf{w}(t) = \frac{\mathbf{h}_L(\mathbf{f}, t)}{N}. \tag{7}$$

To simplify the analysis, we assume that the channels between transmitter and receivers are line-of-sight (LOS) ones. Without loss of generality, we also assume that all channels are corrupted by additive white Gaussian noise (AWGN). Therefore, the received signal at LU can be expressed as

$$\begin{aligned} y_L(t) &= \mathbf{h}_L^H(\mathbf{f}, t)\mathbf{s}(t) + n_L \\ &= \sqrt{\alpha P_s}\mathbf{h}_L^H(\mathbf{f}, t)\mathbf{w}(t)x(t) \\ &\quad + \sqrt{(1-\alpha)P_s}\mathbf{h}_L^H(\mathbf{f}, t)\mathbf{n}_{AN}(t) + n_L \\ &= \sqrt{\alpha P_s}x(t) + n_L, \end{aligned} \tag{8}$$

where n_L is the complex AWGN between the transmitter and LU with a distribution $n_L \sim \mathcal{CN}(0, \sigma_L^2)$. As a result, the SANR at LU is

$$\text{SANR}_L = \frac{\alpha P_s}{\sigma_L^2}. \tag{9}$$

Likewise, the received signal at Eve can be expressed as

$$\begin{aligned} y_E(t) &= \mathbf{h}_E^H(\mathbf{f}, t)\mathbf{s}(t) + n_E \\ &= \sqrt{\alpha P_s}\mathbf{h}_E^H(\mathbf{f}, t)\mathbf{w}(t)x(t) \\ &\quad + \sqrt{(1-\alpha)P_s}\mathbf{h}_E^H(\mathbf{f}, t)\mathbf{n}_{AN}(t) + n_E \end{aligned} \tag{10}$$

where n_E is the complex AWGN between the transmitter and Eve with the distribution $n_E \sim \mathcal{CN}(0, \sigma_E^2)$. From (10), we can see that the aided AN increases the noise energy at Eve since the steering vector of Eve is not orthogonal to the AN project matrix, i.e., $\mathbf{h}_E^H(\mathbf{f}, t)\mathbf{n}_{AN}(t) \neq \mathbf{0}$. In addition, the amplitude and phase of the signals will be distorted by $\sqrt{\alpha P_s}\mathbf{h}_E^H(\mathbf{f}, t)\mathbf{w}(t)$ for $\mathbf{h}_E^H(\mathbf{f}, t)\mathbf{w}(t) \neq 1$. As a result, AN-aided FDA-DM enhances the confidentiality, and the SANR at Eve is given by

$$\text{SANR}_E(t) = \frac{\alpha P_s\left|\mathbf{h}_E^H(\mathbf{f}, t)\mathbf{w}(\mathbf{f}, t)\right|^2}{(1-\alpha)P_s\left|\mathbf{h}_E^H(\mathbf{f}, t)\mathbf{n}_{AN}(t)\right|^2 + \sigma_E^2}. \tag{11}$$

III. THE OPTIMIZATION OF SECRECY CAPACITY FOR THE FDA-DM-AN

We adopt the secrecy capacity as the main performance metric to evaluate the secrecy performance of different schemes. We define the instantaneous secrecy capacity as $C(t) \triangleq \{C_L(t) - C_E(t)\}^+$, where $\{\cdot\}^+ = \max\{\cdot, 0\}$, $C_L(t)$ and $C_E(t)$ are the achievable capacity of LU and Eve at the time t, respectively, which are given by

$$C_L(t) \triangleq \log_2(1 + \text{SANR}_L), \tag{12}$$

and

$$C_E(t) \triangleq \log_2(1 + \mathbb{E}\left[\text{SANR}_E(t)\right]). \tag{13}$$

In order to enhance the secrecy performance of FDA-DM-AN, we maximize the instantaneous secrecy capacity. Mathematically, the objective function can be expressed as

$$\begin{aligned} &\max\ C(t) \triangleq C_L(t) - C_E(t) \\ &\text{s.t.}\ f_m \in [F_{\min}, F_{\max}], \quad \forall m,\ m = 0, 1, ..., N-1. \end{aligned} \tag{14}$$

Utilizing (4)–(13), we rewrite $C(t)$ as

$$\begin{aligned} &C(t) \\ &= \log_2(1 + \frac{\alpha P_s}{\sigma_L^2}) \\ &\quad -\log_2[1 + \frac{\alpha P_s\left|\mathbf{h}_E^H(\mathbf{f}, t)\mathbf{h}_L(\mathbf{f}, t)\right|^2}{(1-\alpha)P_s N^3 \kappa(N^2 - \left|\mathbf{h}_E^H(\mathbf{f}, t)\mathbf{h}_L(\mathbf{f}, t)\right|^2) + \sigma_E^2}]. \end{aligned} \tag{15}$$

where $\kappa \triangleq 1/\mathrm{tr}\left\{\left[N\mathbf{I}_N - \mathbf{h}_L(\mathbf{f},t)\mathbf{h}_L^H(\mathbf{f},t)\right]^2\right\}$. For simplicity, we present the detailed derivation of each terms in (15) in appendix A. Before proceeding to the next step, we define

$$\rho = \mathbf{h}_E^H(\mathbf{f},t)\mathbf{h}_L(\mathbf{f},t). \tag{16}$$

Then, inserting (16) into (15), we obtain

$$C(t) = \log_2(1+\frac{\alpha P_s}{\sigma_L^2}) - \log_2[1+\frac{\alpha P_s \rho^2}{(1-\alpha)P_s N^3 \kappa (N^2-\rho^2)+\sigma_E^2}] \tag{17}$$

It can be easily found that $C(t)$ is monotonically decreasing with ρ^2. Hence, the optimization problem is equivalent to the following expression

$$\begin{aligned} &\min\ \rho^2 \\ &\text{s.t.}\ f_m \in [F_{\min}, F_{\max}], \quad \forall m,\ m=0,1,...,N-1, \end{aligned} \tag{18}$$

Then, $|\rho|$ can be expressed as

$$\begin{aligned} |\rho| &= \left|\mathbf{h}_E^H(\mathbf{f},t)\mathbf{h}_L(\mathbf{f},t)\right| \\ &= \left|\sum_{m=0}^{N-1} e^{j2\pi f_m(\frac{r_L - r_E - md(\sin\theta_L - \sin\theta_E)}{c})}\right| \\ &= \left|\sum_{m=0}^{N-1} e^{j2\pi f_m \psi_m}\right|, \end{aligned} \tag{19}$$

where $\psi_m = \frac{r_L - r_E - md(\sin\theta_L - \sin\theta_E)}{c}$. From (19), we can see that $|\rho|$ is independent of time t. Then, ρ^2 can be expressed as

$$\begin{aligned} \rho^2 &= \left|\mathbf{h}_E^H(\mathbf{f},t)\mathbf{h}_L(\mathbf{f},t)\right|^2 \\ &= \sum_{m=0}^{N-1}\sum_{n=0}^{N-1} e^{j2\pi(f_m\psi_m - f_n\psi_n)} \\ &= \left\{N + \sum_{m=0}^{N-1}\sum_{\substack{n=0\\ n\neq m}}^{N-1} \cos\left[2\pi\ (f_m\psi_m - f_n\psi_n)\right]\right\} \end{aligned} \tag{20}$$

In (20), we can see that the frequency offsets of FDA-DM-AN should be appropriately selected to keep $\mathbf{h}_E(\mathbf{f},t)$ as orthogonal to $\mathbf{h}_L(\mathbf{f},t)$ as possible to get the minimum ρ^2. In the ideal case, we have $\rho^2 = 0$ such that the achievable capacity of Eve is zero. Actually, due to the limited bandwidth, it is generally impossible to guarantee the exact orthogonality between $\mathbf{h}_E(\mathbf{f},t)$ and $\mathbf{h}_L(\mathbf{f},t)$. Therefore, we need to calculate the optimal $\mathbf{f}$ to minimize ρ^2 within the bandwidth. Then, the objective function (20) is equivalent to the following expression

$$\begin{aligned} &\min \sum_{m=0}^{N-1}\sum_{\substack{n=0\\ n\neq m}}^{N-1} \cos\left[2\pi\ (f_m\psi_m - f_n\psi_n)\right] \\ &\text{s.t.}\ f_m \in [F_{\min}, F_{\max}], \quad \forall m,\ m=0,1,...,N-1, \end{aligned} \tag{21}$$

The objective function cannot be solved by ordinary convex methods since it is noncovex and has tightly coupled variables. To tackle this problem, we resort to suboptimal solution of the objective function. According to the characteristics of the target function, the optimization variables can be decomposed into independent blocks, and thus we adopt the block successive upper-bound minimization (BSUM)—an iterative algorithm for convex local approximation of the objective function—to solve the optimization problem [34]. The BSUM algorithm is a very efficient method that can handle such problems with nonconvex objective functions. To facilitate the understanding of our method, we would like to give a brief introduction to the BSUM algorithm.

A. A BRIEF INTRODUCTION OF THE BSUM ALGORITHM

Consider an optimization problem

$$\begin{aligned} &\min\ \mathcal{F}(x_0,...,x_{M-1}) \\ &\text{s.t.}\ x_i \in \mathcal{X}_i,\ i=0,1,...,M-1, \end{aligned} \tag{22}$$

where we assume that the feasible set $\mathcal{X}$ is the Cartesian product of M closed convex sets: $\mathcal{X} = \mathcal{X}_0 \times ... \times \mathcal{X}_{M-1} \subseteq \mathbb{R}^{M\times 1}$, $\mathcal{F}: \prod_{i=0}^{M-1}\mathcal{X}_i \to \mathbb{R}$ is a continuous function. The objective function $\mathcal{F}(\cdot)$ is nonconvex and/or nonsmooth. The BSUM algorithm overcomes this difficulty by optimizing a sequence of approximate objective functions instead, i.e., obtaining the optimal solution by calculating the suboptimal solutions of the approximate objective functions. More specifically, BSUM algorithm starts from a feasible points $\mathbf{x}^0$. At each iteration, the function is minimized for a single block of variables of the approximate objective functions while the rest of the blocks are fixed. The block variable x_i is updated at iteration r by solving the following problem

$$x_i^r = \arg\min_{x_i\in\mathcal{X}_i} u_i(x_i;\mathbf{x}^{r-1}), \quad i=0,1,...,M-1, \tag{23}$$

where $u_i(\cdot)$ is a convex local approximation of the objective function. More precisely, $u_i(\cdot)$ is a global upper-bound convex local approximation of the objective function, which needs to be chosen such that the subproblem (23) is easy to solve.

The suboptimization problem is equivalent to the following expression

$$\begin{aligned} &\min\ u_i(x_i;\mathbf{x}^{r-1}) \\ &\text{s.t.}\ x_i \in \mathcal{X}_i. \end{aligned} \tag{24}$$

In addition, the upper-bound approximation function $u_i(\cdot)$ needs to satisfy the Assumption 1 as following

Assumption 1:

1). $u_i(x_i;\mathbf{x}) = \mathcal{F}(x_i;\mathbf{x});\ \forall x_i \in \mathcal{X}_i, \forall \mathbf{x}\in\mathcal{X}, \forall i$

2). $u_i'(x_i;\mathbf{x},d_i) = \mathcal{F}'(x_i;\mathbf{x},d_i);\ \forall d(0,...,0,d_i,0,...,0)$, s.t. $x_i + d_i \in \mathcal{X}_i, \forall i$

3). $u_i(\mathbf{x}) \geq \mathcal{F}(\mathbf{x}); \forall \mathbf{x}\in\mathcal{X}, \forall i$

4). $u_i(x_i;\mathbf{x})$ is continuous in $(x_i;\mathbf{x}),\ \forall i$.

[34, Th. 2 (a)] ensures the stronger convergence (i.e., it guarantees the iteration generated by the BSUM algorithm to converge a set of stationary points) of the BSUM algorithm. To make every limited point of the iteration generated by the BSUM algorithm be a coordinatewise minimum of (22),

we need the approximation function $u_i(x_i;\mathbf{x})$ to satisfy the following conditions:

1). Suppose that the function $u_i(x_i;\mathbf{x})$ is quasi-convex in x_i, for $i = 0, 1, ...M-1$;
2). The Assumption 1 holds;
3). Assume that the subproblem (24) has a unique solution for any point $\forall \mathbf{x} \in \mathcal{X}$;
4). $\mathcal{F}(\cdot)$ is regular at point $\mathbf{x}$, where $\mathbf{x}$ is a stationary point.

B. A BRIEF REVIEW OF UPPER-BOUND QUADRATIC APPROXIMATION FUNCTION

Based on the above assumptions, we suppose $u_i(x_i)$ is a quadratic function (i.e., $u_i(t) = a_i(t-c_i)^2 + b_i$, where $\{a_i, b_i, c_i\}$ are parameters, and satisfy $a_i \in \mathbb{R}_+$, $b_i \in \mathbb{R}$, and $c_i \in \mathbb{R}$). Then, we give a brief review of the quadratic function. As shown in Fig. 2, the red dash-dot line and the greed dash line denote the situations of $\mathcal{F}'(x_i) = 0$ and $\mathcal{F}'(x_i) \neq 0$, respectively. Suppose the blue solid line is the objective function $\mathcal{F}(x) = \cos[2\pi(fx-\varphi)]$. According to the Assumptions 1 at the point x_i, $\forall i$, we get
If x_i satisfies $\mathcal{F}'(x_i) = 0$,

$$\begin{cases} a_i = (1-b_i)\pi^2 f^2, \\ b_i = \cos[2\pi(fx_i-\varphi)] \in \{-1,+1\}, \\ c_i = x_i, \end{cases} \tag{25}$$

Otherwise,

$$\begin{cases} a_i = \dfrac{-\pi f \sin[2\pi(fx_i-\varphi)]}{x_i - c}, \\ b_i = \cos[2\pi(fx_i-\varphi)] - a(x_i-c)^2, \\ c_i = \begin{cases} \dfrac{\lfloor 2(fx_i-\varphi)\rfloor}{2f} + \dfrac{\varphi}{f} & \text{if } \mathcal{F}'(x_i) > 0, \\ \dfrac{\lceil 2(fx_i-\varphi)\rceil}{2f} + \dfrac{\varphi}{f} & \text{if } \mathcal{F}'(x_i) < 0, \end{cases} \end{cases} \tag{26}$$

where $\lfloor\cdot\rfloor$ and $\lceil\cdot\rceil$ round the argument to the nearest integer towards $-\infty$ and $+\infty$, respectively. Due to rather complicated computation, the detailed derivation processes of (25) and (26) are presented in the Appendix B.

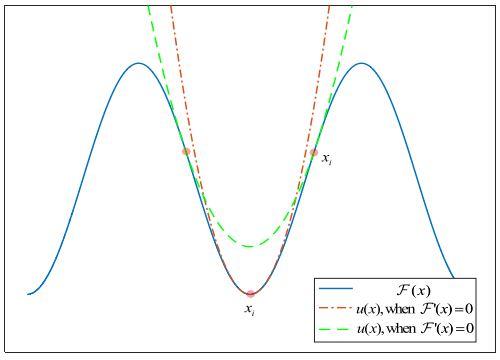

FIGURE 2. Approximating upper bound of the objective function by a convex quadratic function.

C. THE APPLICATION OF BSUM ALGORITHM TO OPTIMIZE FREQUENCY OFFSETS

Based on the above introduction of the BSUM algorithm, we optimize f_m in the rth iteration of objective function as

$$\min \mathcal{F}(f_m;\mathbf{f}^{r-1}) = \sum_{\substack{n=0 \\ n\neq m}}^{N-1} \cos\left[2\pi\left(f_m\psi_m - f_n^{r-1}\psi_n\right)\right]$$
$$\text{s.t. } f_m \in [F_{\min}, F_{\max}], \quad \forall m,\ m = 0, 1, ..., N-1. \tag{27}$$

We define

$$\tilde{\mathcal{F}}_{m,n}(f_m; f_n^{r-1}) \triangleq \cos\left[2\pi\left(f_m\psi_m - f_n^{r-1}\psi_n\right)\right]. \tag{28}$$

Then, inserting (28) into (27), we obtain the rth iteration of objective function as

$$\mathcal{F}(f_m;\mathbf{f}^{r-1}) = \sum_{\substack{n=0 \\ n\neq m}}^{N-1} \tilde{F}_{m,n}(f_m; f_n^{r-1}). \tag{29}$$

Then, $\mathcal{F}(f_m;\mathbf{f}^{r-1})$ is approximated by a upper-bound quadratic function $u_m(\cdot)$. Likewise, we define

$$\tilde{u}_{m,n}(f_m; f_m^{r-1}, f_n^{r-1}) \triangleq a_{m,n}(f_m - c_{m,n})^2 + b_{m,n}, \tag{30}$$

where $a_{m,n} \in \mathbb{R}_+$, $b_{m,n} \in \mathbb{R}$, and $c_{m,n} \in \mathbb{R}$ are parameters of the quadratic function. Therefore, the rth iteration quadratic function $u_m(f_m;\mathbf{f}^{r-1})$ is expressed as

$$u_m(f_m;\mathbf{f}^{r-1}) = \sum_{\substack{n=0 \\ n\neq m}}^{N-1} \tilde{u}_{m,n}(f_m; f_m^{r-1}, f_n^{r-1}). \tag{31}$$

According to the Assumption 1, the upper-bound quadratic function $u_m(\cdot)$ satisfies the following equations

1). $\tilde{u}_{m,n}(f_m^{r-1}; f_m^{r-1}, f_n^{r-1}) = \tilde{\mathcal{F}}_{m,n}(f_m^{r-1}; f_n^{r-1})$,
2). $\tilde{u}'_{m,n}(f_m^{r-1}; f_m^{r-1}, f_n^{r-1}) = \tilde{\mathcal{F}}'_{m,n}(f_m^{r-1}; f_n^{r-1})$,
3). $\tilde{u}_{m,n}(f_m^{r-1}; f_m^{r-1}, f_n^{r-1}) \geq \tilde{\mathcal{F}}_{m,n}(f_m^{r-1}; f_n^{r-1})$,
4). $\left|c_{m,n} - f_m^{r-1}\right| < \dfrac{1}{2\psi_m}$,

In addition,

$$\tilde{\mathcal{F}}'_{m,n}(f_m^{r-1}; f_n^{r-1}) = -2\pi\psi_m \sin\left[2\pi\left(f_m^{r-1}\psi_m - f_n^{r-1}\psi_n\right)\right] \tag{32}$$

Based on the above knowledge of upper-bound quadratic function for solving $\{a_{m,n}, b_{m,n}, c_{m,n}\}$, we obtain the parameters as follows
If f_m^{r-1} satisfies $\mathcal{F}'(f_m^{r-1}; f_n^{r-1}) = 0$,

$$\begin{cases} a_{m,n} = \left(1-b_{m,n}\right)\pi^2\psi_m^2, \\ b_{m,n} = \cos\left[2\pi\left(f_m^{r-1}\psi_m - f_n^{r-1}\psi_n\right)\right] \in \{-1,+1\}, \\ c_{m,n} = f_m^{r-1}, \end{cases} \tag{33}$$

Otherwise,

$$\begin{cases} a_{m,n} = \dfrac{-\pi\psi_m \sin\left[2\pi\left(f_m^{r-1}\psi_m - f_n^{r-1}\psi_n\right)\right]}{f_m^{r-1} - c_{m,n}}, \\ b_{m,n} = \cos\left[2\pi\left(f_m^{r-1}\psi_m - f_n^{r-1}\psi_n\right)\right] \\ \qquad -a_{m,n}\left(f_m^{r-1} - c_{m,n}\right)^2, \\ c_{m,n} = \begin{cases} \dfrac{\lfloor 2\left(f_m^{r-1}\psi_m - f_n^{r-1}\psi_n\right)\rfloor}{2\psi_m} + \dfrac{f_n^{r-1}\psi_n}{\psi_m}, \\ \qquad \text{if } \mathcal{F}'_{m,n}(f_m^{r-1}) > 0 \\ \dfrac{\lceil 2\left(f_m^{r-1}\psi_m - f_n^{r-1}\psi_n\right)\rceil}{2\psi_m} + \dfrac{f_n^{r-1}\psi_n}{\psi_m}, \\ \qquad \text{if } \mathcal{F}'_{m,n}(f_m^{r-1}) < 0 \end{cases} \end{cases} \tag{34}$$

Now, we can obtain the optimal solution by calculating the suboptimal solutions of the upper-bound quadratic function. The optimization problem (27) can be recast as

$$\begin{aligned} &\min \sum_{\substack{n=0 \\ n\neq m}}^{N-1} a_{m,n}(f_m - c_{m,n})^2 + b_{m,n} \\ &\text{s.t.} f_m \in [F_{\min}, F_{\max}], \quad \forall m,\ m = 0, 1, ..., N-1. \end{aligned} \tag{35}$$

To solve (35), let $f_m^r = \arg\min_{f_m^r \in [F_{\min}, F_{\max}]} u_m(f_m; \mathbf{f}^{r-1})$, and thus the optimal solution can be expressed as

$$f_m^r = \frac{\sum_{\substack{n=0 \\ n\neq m}}^{N-1} a_{m,n}c_{m,n}}{\sum_{\substack{n=0 \\ n\neq m}}^{N-1} a_{m,n}} \in [F_{\min}, F_{\max}]. \tag{36}$$

In summary, the detailed pseudocode of BSUM algorithm is given in Algorithm 1.

Algorithm 1 Iterative BSUM Approach to Optimal Solution of (27)

1: Pick up an initial point $\mathbf{f}^0 \in [F_{\min}, F_{\max}]$ and set $r = 0$, $m = 0$;
2: $r = r + 1, m = (r \mod N) + 1$;
3: Substitute $\mathbf{f}^{r-1}$ into (33) or (34) to get $\{a_{m,n}, b_{m,n}, c_{m,n}\}$;
4: Substitute $\{a_{m,n}, b_{m,n}, c_{m,n}\}$ into (36) to get f_m^r;
5: Set $f_m^r = f_n^{r-1}$, $\forall n \neq m$;
6: **If** $r <$ the max iteration times or $\|\mathbf{f}^r - \mathbf{f}^{r-1}\| \geq \varepsilon$, go to the step 2;
7: **Otherwise stop**. Get the finally optimal $\mathbf{f}^r$;

D. SOLUTION TO AVERAGE TIME-INVARIANT PROBLEM

In the previous discussion, we know that optimal frequency offsets are independent of time, but the beamforming vector and AN are instantaneous problem, which means the secrecy capacity will change with time and brings a large budget to implement. Now we maximize the average secrecy capacity within a predefined time period of length T is expressed as

$$\begin{aligned} &\max \frac{1}{T}\int_0^T C(t)dt \\ &\text{s.t.} f_m \in [F_{\min}, F_{\max}], \quad \forall m,\ m = 0, 1, ..., N-1. \end{aligned} \tag{37}$$

In order to keep the secrecy capacity time-invariant, we need to update $\mathbf{w}(t)$ and $\mathbf{n}_{AN}(t)$ with time. It is generally impractical to continuously update the beamforming vector and AN. As a compromise, we define some time interval as $\Delta T_w = \frac{T}{L}$, and thus a series of beamforming vector and AN updating time points are $t_l^w = l\Delta T_w$, $l = 0, 1, ..., L-1$. That is, we update beamforming vector and AN at t_l^w and then use $\mathbf{w}(t_l^w)$ and $\mathbf{n}_{AN}(t_l^w)$ as discrete beamforming vector and AN within $t_l^w \leq t \leq t_{l+1}^w$. Thus, we obtain

$$\begin{aligned} &\frac{1}{T}\int_0^T C(t)dt \\ &\simeq \frac{1}{T}\sum_{l=0}^{L-1}\int_{t_l^w}^{t_{l+1}^w} \{\log_2[1 + \frac{\alpha P_s\left|\mathbf{h}_L^H(\mathbf{f}, t)\mathbf{w}(t_l^w)\right|^2}{(1-\alpha)P_s\left|\mathbf{h}_L^H(\mathbf{f}, t)\mathbf{n}_{AN}(t_l^w)\right|^2 + \sigma_L^2}] \\ &\quad -\log_2[1 + \frac{\alpha P_s\left|h_E^H(\mathbf{f}, t)\mathbf{w}(t_l^w)\right|^2}{(1-\alpha)P_s\left|\mathbf{h}_E^H(\mathbf{f}, t)\mathbf{n}_{AN}(t_l^w)\right|^2 + \sigma_E^2}]\}dt. \end{aligned} \tag{38}$$

IV. FDA-DM-AN FOR MULTI-EVES SYSTEM

Without loss of generality, there may exist several Eves wiretapping the confidential signal. In this section, we extend the proposed approach to the case of multi-Eves, i.e., assuming the number of Eve is K, $K > 1$. Just like the method proposed above, the multi-Eves optimization problem based on FDA-DM-AN is formulated as

$$\begin{aligned} &\max\ C(t) = C_L(t) - \tilde{C}_E(t) \\ &\text{s.t.} f_m \in [F_{\min}, F_{\max}], \quad \forall m,\ m = 0, 1, ..., N-1, \end{aligned} \tag{39}$$

where $\tilde{C}_E(t) \triangleq \log_2(1 + \sum_{i=0}^{K-1} v_i \mathbb{E}[\text{SANR}_{E_i}(t)])$. Define the normalized weighted vector as $\mathbf{v} \triangleq [v_0, v_1, ...v_{K-1}]^T$, where v_i is the weight of the ith Eve, and satisfies $v_0 + v_1 + \ldots + v_{K-1} = 1$. Similarly, the objective function (39) is given by

$$\begin{aligned} &C(t) \\ &= \log_2(1 + \frac{\alpha P_s}{\sigma_L^2}) - \log_2 \\ &\quad \times (1 + \sum_{i=0}^{K-1} \frac{v_i\alpha P_s\left|\mathbf{h}_{E_i}^H(\mathbf{f}, t)\mathbf{h}_L(\mathbf{f}, t)\right|^2}{(1-\alpha)P_s N^3\kappa(N^2 - \left|\mathbf{h}_{E_i}^H(\mathbf{f}, t)\mathbf{h}_L(\mathbf{f}, t)\right|^2) + \sigma_{E_i}^2}) \end{aligned} \tag{40}$$

where $\kappa \triangleq 1/\text{tr}\left\{\left[N\mathbf{I}_N - \mathbf{h}_L(\mathbf{f}, t)\mathbf{h}_L^H(\mathbf{f}, t)\right]^2\right\}$. Likewise, we define

$$\rho_i \triangleq \mathbf{h}_{E_i}^H(\mathbf{f}, t)\mathbf{h}_L(\mathbf{f}, t). \tag{41}$$

Then, inserting (41) into (40), the optimization secrecy capacity is given by

$$\begin{aligned}&\max\ C(t)=\log_2(1+\frac{\alpha P_s}{\sigma_L^2})\\&\quad-\left[\log_2(1+\sum_{i=0}^{K-1}\frac{v_i\alpha P_s\rho_i^2}{(1-\alpha)P_sN^3\kappa(N^2-\rho_i^2)+\sigma_{E_i}^2})\right]\\&\text{s.t.}\ f_m\in[F_{\min},F_{\max}],\quad \forall m,\ m=0,1,...,N-1.\end{aligned}\tag{42}$$

Likewise, $C(t)$ is monotonically decreasing with $\sum_{i=0}^{K-1} v_i\rho_i^2$ when $\rho_i^2\to 0$. The optimization problem (42) is equivalent to the following expression

$$\begin{aligned}&\min\ \sum_{i=0}^{K-1}v_i\rho_i^2\\&\text{s.t.}\ f_m\in[F_{\min},F_{\max}],\quad \forall m,\ m=0,1,...,N-1.\end{aligned}\tag{43}$$

Then, $\sum_{i=0}^{K-1} v_i\rho_i^2$ can be expressed as

$$\begin{aligned}&\sum_{i=0}^{K-1}v_i\rho_i^2\\&=\sum_{i=0}^{K-1}\sum_{m=0}^{N-1}\sum_{n=0}^{N-1}v_ie^{j2\pi\left(f_m\psi_m^i-f_n\psi_n^i\right)}\\&=\left\{NK+\sum_{i=0}^{K-1}\sum_{m=0}^{N-1}\sum_{\substack{n=0\\n\neq m}}^{N-1}v_i\cos\left[2\pi\left(f_m\psi_m^i-f_n\psi_n^i\right)\right]\right\}.\end{aligned}\tag{44}$$

where $\psi_m^i=\frac{r_L-r_{E_i}-md(\sin\theta_L-\sin\theta_{E_i})}{c}$. Hence, the multi-Eves optimization problem is equivalent to the following expression

$$\begin{aligned}&\min\ \sum_{i=0}^{K-1}\sum_{m=0}^{N-1}\sum_{\substack{n=0\\n\neq m}}^{N-1}v_i\cos\left[2\pi\left(f_m\psi_m^i-f_n\psi_n^i\right)\right]\\&\text{s.t.}\ f_m\in[F_{\min},F_{\max}],\quad \forall m,\ m=0,1,...,N-1.\end{aligned}\tag{45}$$

Then, in the same manner, (45) can be solved by BSUM algorithm.

V. NUMERICAL RESULTS AND ANALYSIS

In this section, the parameters and specifications in our simulations are used as follows. Suppose that both LU and Eve are a single-antenna receiver. Define bandwidth as $B_w\triangleq F_{\max}-F_{\min}$. An N-element uniformly-spaced linear array using is otropic elements with a spacing of $d=\lambda_0/2$ operating at a reference frequency $f_0=1$ GHz is considered in the transmitter. We consider the secrecy capacity upper bound—the maximum secrecy capacity in the case of no Eve, i.e., $C_{\max}=\log_2(1+\mathrm{SNR}_L)$=$\log_2(1+\alpha P_s/\sigma_L^2)$. We compare secrecy capacity of different DM schemes—line FDA-DM-AN (L-FDA-DM-AN), i.e., $f_m=f_0+m\Delta f$, $m=0,1,...N-1$, R-FDA-DM-AN, i.e., $f_m=f_0+\eta\Delta f$, where η is a random variable, logarithmic FDA-DM-AN (log-FDA-DM-AN), i.e., $f_m=f_0+\log(m+1)\Delta f$, $m=0,1,\ldots N-1$, PA-DM-AN, i.e., Δf=0, and our proposed optimization method. In addition, we plot the secrecy capacity distribution to evaluate the performance in different scenarios.

A. FDA-MD-AN FOR SINGLE PROXIMAL EVE

In the case of a single Eve, we assume channel noise power of both LU and Eve are identical to 0 dBm (i.e., $\sigma_L^2=\sigma_E^2=1$). We fix the location of the LU at (1200 m, 30°). As we know, the beam steering of PA-DM is independent of the range. In order to highlight the range-angle dependent beampattern of FDA-DM, we consider two cases: 1). The LU and Eve are located at the same direction, whereas the range between Eve and LU is proximal, i.e., $(r_E,\theta_E)=(1300\text{ m},30°)$; 2). Both angle and range are proximal between LU and Eve, i.e., $(r_E,\theta_E)=(1300\text{ m},32°)$.

Fig. 3 plots the convergence of the BSUM algorithm. Initial points are chosen from random points. In this case, Eve's location is $(r_E,\theta_E)=(1300\text{ m},30°)$ and LU's location is $(r_L,\theta_L)=(1200\text{ m},30°)$, $N=32$, and $B_w=4$ MHz. From Fig. 3 (a) and (b), it can be seen that the algorithm can get stable frequency offsets, and the objective function reaches minimum values in about 8 iterations.

In the next scenario, we compare the secrecy capacity of different DM schemes in the same message bandwidth. We can get the maximum secrecy capacity when power and power allocation factor are fixed, i.e., $C_{\max}=7.972$ when

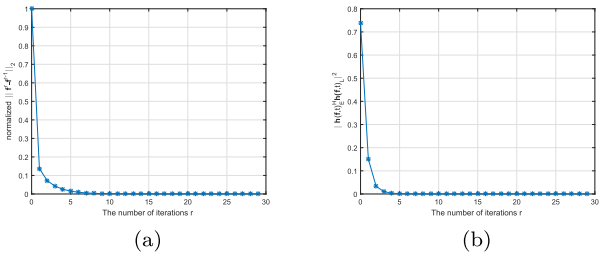

FIGURE 3. The convergence of BSUM iterations (a) The normalized $\left\|\mathbf{f}^r-\mathbf{f}^{r-1}\right\|_2$ versus the number of iterations r. (b) $\left|\mathbf{h}_E^H(\mathbf{f},t)\mathbf{h}_L(\mathbf{f},t)\right|^2$ versus the number of iterations r.

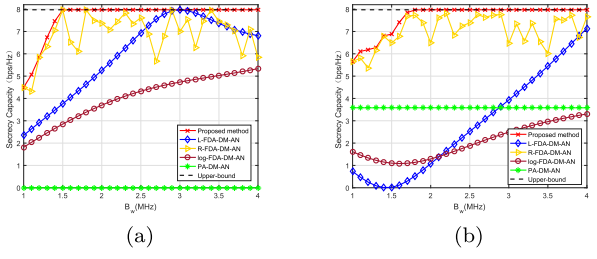

FIGURE 4. The secrecy capacity comparison for different DM schemes versus B_W, where $P_S=500$ W, $\alpha=0.5$, $N=32$, and LU's location is (1200 m,30°) (a) Eve's location is (1300 m,30°), (b) Eve's location is (1300 m,32°).

$P_s = 500$ W, $\alpha = 0.5$. Fig. 4 shows that the secrecy capacity of the proposed method is much higher than that of others since the frequency offsets are optimized. Specifically, the proposed method can achieve the upper bound when B_W is large enough. The secrecy capacity of the R-FDA-DM-AN is unstable since the frequency offsets are randomly chosen. Moreover, the secrecy capacity of the L-FDA-DM-AN scheme displays cyclic variations. The secrecy capacity of log-FDA-DM-AN is the lowest. As shown in Fig. 4 (a), the secrecy capacity of the PA-DM-AN scheme is zero when Eve locates in the same direction as LU relative to the transmitter. It can be seen from Fig. 4 (b), as expected, the secrecy capacity of the PA-DM-AN scheme has a few improvements when there exist angle difference between Eve and LU.

In Fig. 5 and 6, we illustrate how the values of power allocation factor α and power P_s influence the secrecy capacity among the different DM schemes. Similarly, the proposed approach outperforms the conventional DM approach. The secrecy capacity of the R-FDA-DM-AN is unstable. As expected, in Fig. 5 (a) and Fig. 6 (a), it can be seen that the secrecy capacity of the PA-DM-AN scheme is zero at any α and P_s when the angle of Eve is same as the LU's. Similarly, the secrecy capacity of the PA-DM-AN scheme has an improvement when there exists angle proximity.

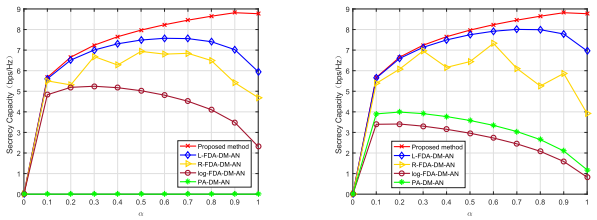

(a) (b)

FIGURE 5. The secrecy capacity comparison for different DM schemes versus α, where $B_W = 4$ MHz, $P_S = 500$ W, $N = 32$, LU's location is (1200 m,30°) (a) Eve's location is (1300 m,30°), (b) Eve's location is (1300 m,32°).

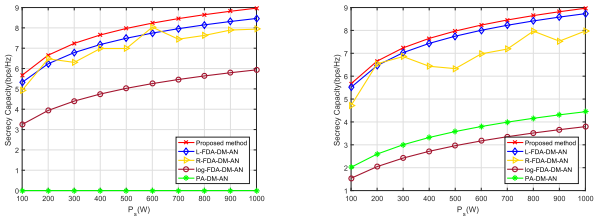

(a) (b)

FIGURE 6. The secrecy capacity comparison for different DM schemes versus P_S, where $B_W = 4$ MHz, $\alpha = 0.5$, $N = 32$, LU's location is (1200 m, 30°) (a) Eve's location is (1300 m,30°), (b) Eve's location is (1300 m,32°).

Fig. 7 shows the secrecy capacity distribution of the proposed method versus Eve's angle and range when the number of antenna elements in an array is set as 32 and 256, respectively. Two conclusions can be obtained: Firstly, the secrecy

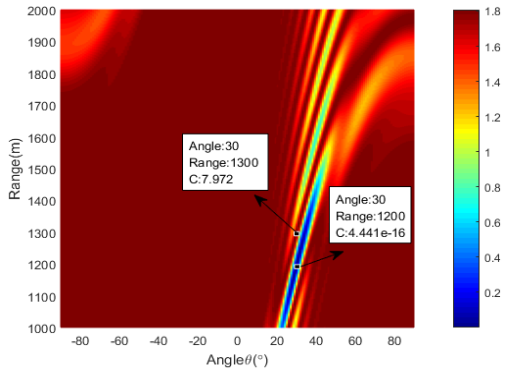

(a)

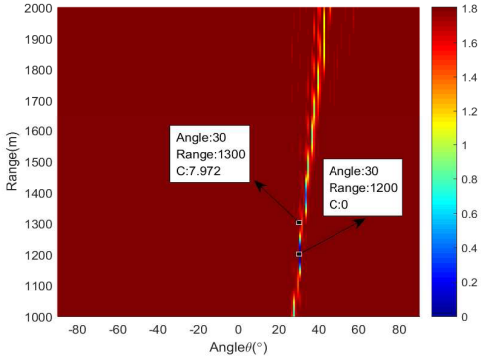

(b)

FIGURE 7. The secrecy capacity distribution of the proposed method versus Eve's angle-range, where $B_W = 4$ MHz, $P_S = 500$ W, $\alpha = 0.5$, LU's location is (1200 m,30°) and Eve's location is (1300 m,30°), (a) $N = 32$, (b) N=256.

capacity is approximately zero only when the Eve locates at (1200 m, 30°) that is the location of LU. Meanwhile, at other points, especially the position of Eve (1300 m, 30°), the secrecy capacity approaches the upper bound $C_{\max}$, which means the proposed method can realize physical layer security communication for proximal LU and Eve. Secondly, increasing the number of antennas improves the array degrees of freedom to help decouple the direction and range of FDA-DM-AN. Therefore, higher secrecy performance can be achieved.

To show the decoupling between the direction and range of FDA-DM-AN more clearly, we further plot normalized secrecy capacity (dB) of the proposed method versus angle and range, respectively, as shown in Fig. 8. It can be observed that unique minimum secrecy capacity occurs at (1200 m, 30°).

Fig. 9 demonstrates the secrecy capacity distribution of L-FDA-DM-AN versus Eve's location angle-range when the element of linear antenna array is set as 32 and 256, respectively. The results illustrate that the L-FDA-DM-AN has a serious coupled problem no matter how many antennas are employed, which seriously affects the secrecy performance in wireless communications.

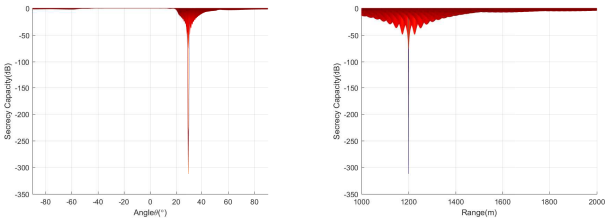

(a) (b)

FIGURE 8. Normalized secrecy capacity (dB) of the proposed method versus (a) Eve's angle, (b) Eve's range, where $B_W = 4$ MHz, $P_S = 500$ W, $\alpha = 0.5$, $N = 32$, LU's location is (1200 m,30°) and Eve's location is (1300 m,30°).

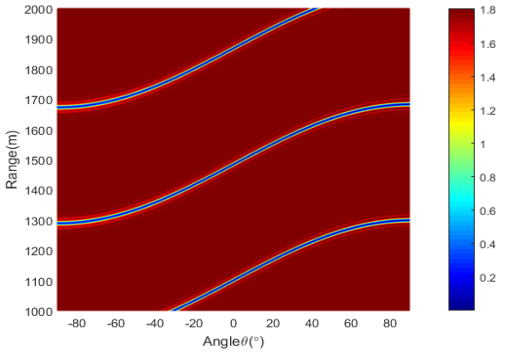

(a)

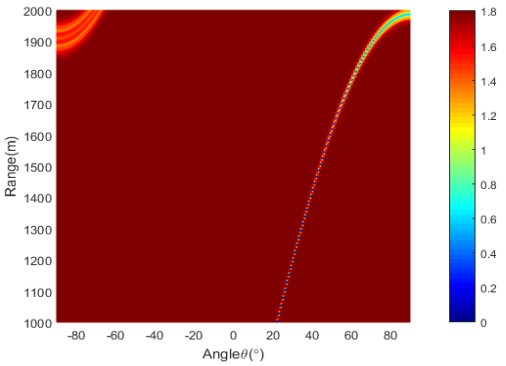

(b)

FIGURE 9. The secrecy capacity distribution of L-FDA-DM-AN versus Eve's angle-range, where $B_W = 4$ MHz, $P_S = 500$ W, $\alpha = 0.5$, LU's location is (1200 m,30°) and Eve's location is (1300 m,30°), (a) $N = 32$, (b) $N = 256$.

Similarly, in order to show the coupled problem more clearly, the normalized secrecy capacity (dB) versus Eve's angle and Eve's range of L-FDA-DM-AN is illustrated in Fig. 10. Compared with Fig. 8, it can be clearly found that except the location (1200 m,30°), there are some others locations, especially nearby (1600 m,30°) and (2000 m,30°), where Eve can receive confidential information. As a result, the wireless security communication suffers from the severe performance degradation.

Next, we show the the secrecy capacity distribution of the proposed method, where the locations of LU and Eve are set

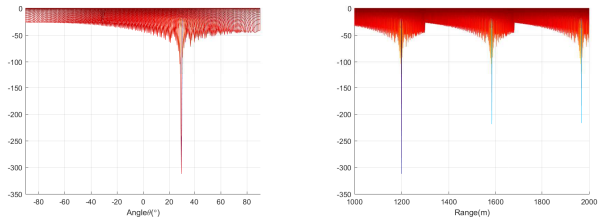

(a) (b)

FIGURE 10. Normalized secrecy capacity (dB) of L-FDA-DM-AN versus (a) Eve's angle, (b) Eve's range, where $B_W = 4$ MHz, $P_S = 500$ W, $\alpha = 0.5$, $N = 32$, LU's location is (1200 m,30°) and Eve's location is (1300 m,30°).

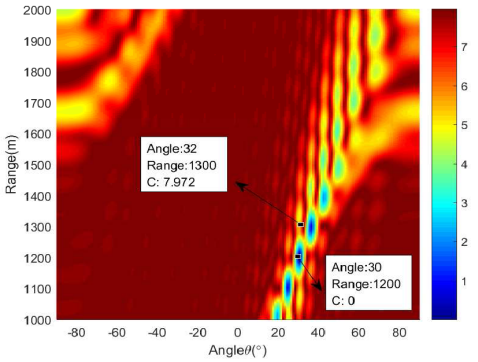

FIGURE 11. The secrecy capacity distribution of the proposed method versus Eve's angle-range, where $B_W = 4$ MHz, $P_S = 500$ W, $\alpha = 0.5$, $N = 32$, LU's location is (1200 m,30°), Eve's location is (1300 m,32°).

as $(r_L, \theta_L) = (1200\text{ m}, 30°)$ and $(r_E, \theta_E) = (1300\text{ m}, 32°)$, respectively. It can be seen from Fig. 11, the secrecy capacity is almost zero only when Eve locates at (1200 m, 30°), whereas at other points, especially location of (1300 m, 32°), the secrecy capacity approaches the upper bound. All of the results above show that the proposed method is valid for both angle and range dimensions.

To show the behavior of time-invariant FDA beamforming in practice, we define steering vector updating time interval as $\Delta T_s \triangleq \frac{\Delta T_w}{J}$, $J \gg 1$, where ΔT_w is the updating time interval of beamforming vector and AN. The steering vector updating time points are $t^s_{l,j} = t^w_{l,j} + j\Delta T_s$, for $j = 0, 1, .., J-1$. Therefore, the average secrecy capacity can be approximated by

$$\begin{aligned}
&\frac{1}{T}\int_0^T C(t)dt \\
&\simeq \frac{1}{T}\sum_{l=0}^{L-1}\sum_{j=0}^{J-1}\Delta T_s \\
&\cdot[\log_2(1+\frac{\alpha P_s\left|\mathbf{h}_L^H(\mathbf{f}, t^s_{l,j})\mathbf{w}(t^w_l)\right|^2}{(1-\alpha)P_s\left|\mathbf{h}_L^H(\mathbf{f}, t^s_{l,j})\mathbf{n}_{AN}(t^w_l)\right|^2+\sigma_L^2}) \\
&-\log_2(1+\frac{\alpha P_s\left|\mathbf{h}_E^H(\mathbf{f}, t^s_{l,j})\mathbf{w}(t^w_l)\right|^2}{(1-\alpha)P_s\left|\mathbf{h}_E^H(\mathbf{f}, t^s_{l,j})\mathbf{n}_{AN}(t^w_l)\right|^2+\sigma_E^2}]
\end{aligned} \tag{46}$$

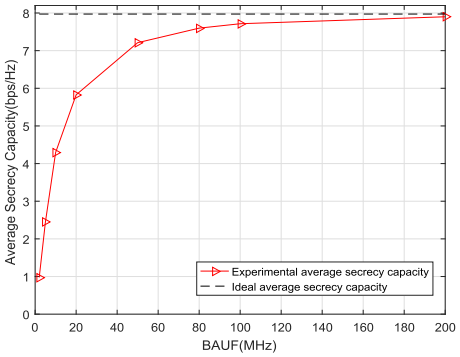

FIGURE 12. The average secrecy capacity versus BAUF, where $B_W = 4$ MHz, $\alpha = 0.5$, $P_s = 500$ W, and $N = 32$.

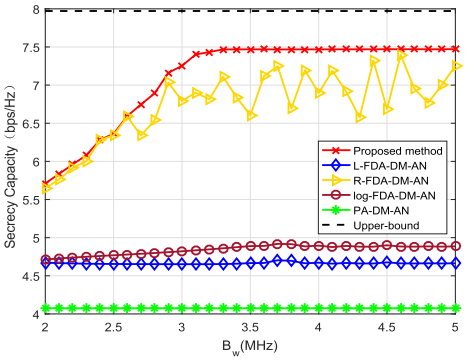

FIGURE 13. The secrecy capacity comparison for different DM schemes versus B_W, where $P_s = 500$ W, $\alpha = 0.5$, and $N = 32$.

Fig.12 exhibits the average secrecy capacity of FDA-DM-AN with different beamforming vector and AN update frequencies (BAUF). We assume a predefined time period of length $T = 20\mu s$ and set the steering vector update frequency as 200 GHz. Without loss of generality, there is a tradeoff between secrecy capacity and implementation cost. It can be seen clearly from Fig.12, the resultant average secrecy capacity is very close to that of the ideal update frequency when $BAUF = 80$ MHz, which can be easily implemented in practice.

B. FDA-MD-AN FOR PROXIMAL MULTI-EVES

Next, we consider the case of multi-Eves. Similar to the case of single-Eve, we evaluate the secrecy capacity of different DM schemes with the change of bandwidth, power allocation factor, and power. Besides, we show the secrecy capacity distribution of the proposed method versus Eve's angle and range. We consider the system that consists of four Eves (i.e., $K = 4$). Assume that the channel noise power is 0 dBm for all Eves and LU (i.e., $\sigma_L^2 = \sigma_{E_k}^2 = 1, k = 0, 1, 2, 3$). In order to present the characteristics of FDA-MD (range-angle dependence) and satisfy the condition of proximal LU and Eves, the location of LU is set as $(r_L, \theta_L) = (1200\text{ m}, 30°)$, and the locations of Eves are set as $(r_{E_0}, \theta_{E_0}) = (1300\text{ m}, 35°)$, $(r_{E_1}, \theta_{E_1}) = (1150\text{ m}, 25°)$, $(r_{E_2}, \theta_{E_2}) = (1200\text{ m}, 35°)$, and $(r_{E_3}, \theta_{E_3}) = (1250\text{ m}, 30°)$. We set $v_0 = v_1 = 0.1, v_2 = v_3 = 0.4$ to strengthen the secrecy performance of the second and third Eve due to only one dimension difference.

In Fig. 13, we compare the secrecy capacity of different DM schemes with the change of bandwidth. It can be clearly seen that the proposed method cannot reach the upper bound since it is impossible to make exactly orthogonal between the steering vectors of multi-Eves and that of LU with the limited bandwidth, but the secrecy capacity of the proposed method is much better than that of other DM schemes. The secrecy capacity of the R-FDA-DM-AN fluctuates with the bandwidths, and the secrecy capacities of log-FDA-DM-AN, L-FDA-DM-AN, and PA-DM-AN are low.

Assuming that the allocation factor varies from $\alpha = 0$ to $\alpha = 1$ and the power varies from $P_s = 100$ W to $P_s = 1000$ W, gradually, we study their influence on the

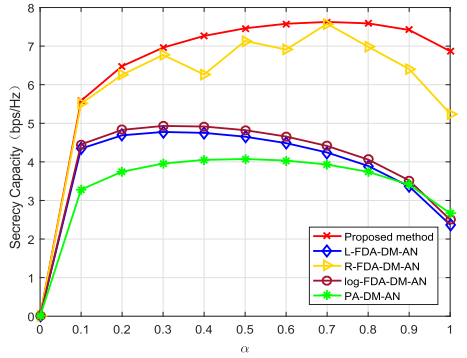

FIGURE 14. The secrecy capacity comparison for different DM schemes versus α, where $B_W = 4$ MHz, $P_s = 500$ W, and $N = 32$.

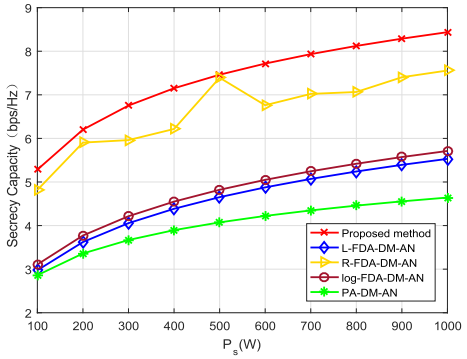

FIGURE 15. The secrecy capacity comparison for different DM schemes versus P_s, where $B_W = 4$ MHz, $\alpha = 0.5$, and $N = 32$.

secrecy capacity. The results in Fig. 14 and 15 indicate that the proposed method outperforms the conventional DM approaches. As expected, the R-FDA-DM-AN can not guarantee high confidentiality. The secrecy capacities of L-FDA-DM-AN, PA-DM-AN, and log-FDA-DM-AN are low.

In the last simulation, we show the secrecy capacity distribution of the proposed method versus Eve's angle and range. From Fig. 17, it can be seen that the secrecy capacity is nearly zero at the location of LU (1200 m, 30°), and all of the secrecy capacities are closed to the upper bound at the locations of Eves. Therefore, the aforementioned observations intuitively demonstrate the advantages of the proposed scheme.

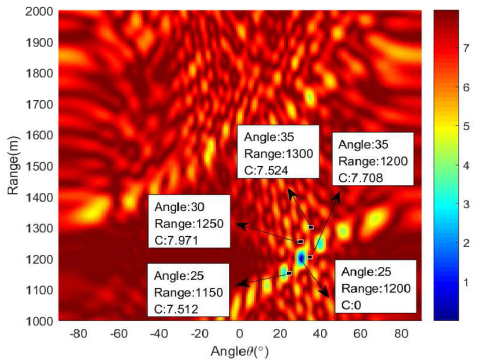

FIGURE 16. The secrecy capacity distribution of the proposed method versus Eve's angle-range, where $B_W = 4$ MHz, $P_s = 500$ W, $\alpha = 0.5$, and $N = 32$.

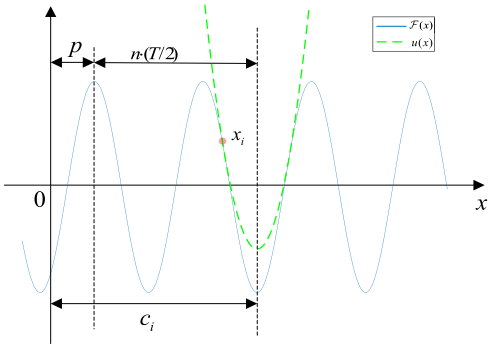

FIGURE 17. Approximating of the objective function by an upper-bound quadratic function, when $\mathcal{F}'(x_i) < 0$.

VI. CONCLUSION

In this paper, we apply a DM scheme based on frequency diverse arrays with artificial noise to enhance the security of wireless communications. In order to guarantee the security of proximal LU and Eve, we maximize the secrecy capacity by optimizing the frequency offsets across the array antennas, and then efficiently solve such an optimization problem by BSUM algorithm. Moreover, we extend the proposed scheme to the case of multi-Eves. Finally, the effectiveness of the proposed scheme has been verified via extensive numerical simulations. Numerical results show that :1) The proposed method is more secure than other DM approaches with the change of bandwidth, power allocation factor, and power; 2) The proposed scheme can decouple the correlation between the direction and range, which can enhance the security of wireless communications; 3) It is feasible to use a BAUF implemented easily in practice to achieve time-invariant secure communications; 4) The proposed optimal method also has satisfactory security performance in the case of multi-Eves.

APPENDIX A
DERIVATION OF THE SECRECY CAPACITY $C(x)$

Inserting (9), (11), (12), and (13) into $C(t)$, we obtain

$$\begin{aligned} C(t) &= C_L(t) - C_E(t) \\ &= \log_2(1 + \mathrm{SANR}_L) \\ &\quad - \log_2(1 + \mathbb{E}[\mathrm{SANR}_E(t)]) \\ &= \log_2(1 + \frac{\alpha P_s}{\sigma_L^2}) \\ &\quad - \log_2(1 + \frac{\alpha P_s \left|\mathbf{h}_E^H(\mathbf{f},t)\mathbf{w}(t)\right|^2}{(1-\alpha)P_s\mathbb{E}\left[\left|\mathbf{h}_E^H(\mathbf{f},t)\mathbf{n}_{AN}(t)\right|^2\right] + \sigma_E^2}). \end{aligned} \tag{47}$$

Then, inserting (7) into (47), we obtain

$$\begin{aligned} C(t) &= \log_2(1 + \frac{\alpha P_s}{\sigma_L^2}) \\ &\quad - \log_2(1 + \frac{\alpha P_s \left|\mathbf{h}_E^H(\mathbf{f},t)\mathbf{h}_L(\mathbf{f},t)\right|^2}{(1-\alpha)P_s N^2 \mathbb{E}\left[\left|\mathbf{h}_E^H(\mathbf{f},t)\mathbf{n}_{AN}(t)\right|^2\right] + \sigma_E^2}). \end{aligned} \tag{48}$$

Next, using (4) and (5), and based on $\mathbf{z} \sim \mathcal{CN}(0, \mathbf{I}_N)$, i.e., $\mathbb{E}[\mathbf{z}\mathbf{z}^H] = \mathbf{I}_N$, the denominator $\mathbb{E}\left[\left|\mathbf{h}_E^H(\mathbf{f},t)\mathbf{n}_{AN}(t)\right|^2\right]$ is given by

$$\begin{aligned} &\mathbb{E}\left[\left|\mathbf{h}_E^H(\mathbf{f},t)\mathbf{n}_{AN}(t)\right|^2\right] \\ &= \frac{\mathbb{E}\left[\mathbf{h}_E^H(\mathbf{f},t)\mathbf{P}_{AN}(t)\mathbf{z}\mathbf{z}^H\mathbf{P}_{AN}^H(t)\mathbf{h}_E(\mathbf{f},t)\right]}{\mathbb{E}\left[\|\mathbf{P}_{AN}(t)\mathbf{z}\|_2^2\right]} \\ &= \frac{\mathbf{h}_E^H(\mathbf{f},t)\mathbf{P}_{AN}(t)\mathbb{E}\left[\mathbf{z}\mathbf{z}^H\right]\mathbf{P}_{AN}^H(t)\mathbf{h}_E(\mathbf{f},t)}{\mathrm{tr}\left\{\mathbf{P}_{AN}(t)\mathbb{E}\left[\mathbf{z}\mathbf{z}^H\right]\mathbf{P}_{AN}^H(t)\right\}} \\ &= \frac{\mathbf{h}_E^H(\mathbf{f},t)\mathbf{P}_{AN}(t)\mathbf{I}_N\mathbf{P}_{AN}^H(t)\mathbf{h}_E(\mathbf{f},t)}{\mathrm{tr}\left\{\mathbf{P}_{AN}(t)\mathbf{I}_N\mathbf{P}_{AN}^H(t)\right\}} \\ &= \frac{N - \frac{\left|\mathbf{h}_E^H(\mathbf{f},t)\mathbf{h}_L(\mathbf{f},t)\right|^2}{N}}{\mathrm{tr}\left\{\left[\mathbf{I}_N - \frac{\mathbf{h}_L(\mathbf{f},t)\mathbf{h}_L^H(\mathbf{f},t)}{N}\right]^2\right\}} \\ &= \frac{N\left(N^2 - \left|\mathbf{h}_E^H(\mathbf{f},t)\mathbf{h}_L(\mathbf{f},t)\right|^2\right)}{\mathrm{tr}\left\{\left[N\mathbf{I}_N - \mathbf{h}_L(\mathbf{f},t)\mathbf{h}_L^H(\mathbf{f},t)\right]^2\right\}}. \end{aligned} \tag{49}$$

Then, inserting (49) into (48), we obtain

$$\begin{aligned} C(t) &= \log_2(1 + \frac{\alpha P_s}{\sigma_L^2}) \\ &\quad - \log_2[1 + \frac{\alpha P_s \left|\mathbf{h}_E^H(\mathbf{f},t)\mathbf{h}_L(\mathbf{f},t)\right|^2}{(1-\alpha)P_s N^3 \kappa (N^2 - \left|\mathbf{h}_E^H(\mathbf{f},t)\mathbf{h}_L(\mathbf{f},t)\right|^2) + \sigma_E^2}], \end{aligned} \tag{50}$$

where $\kappa \triangleq 1/\mathrm{tr}\left\{\left[N\mathbf{I}_N - \mathbf{h}_L(\mathbf{f},t)\mathbf{h}_L^H(\mathbf{f},t)\right]^2\right\}$.

APPENDIX B
DERIVATION OF THE PARAMETERS $\{a_i, b_i, c_i\}$

According to the upper-bound quadratic function $u_i(\cdot)$ needs to satisfy Assumption 1,

If x_i satisfies $\mathcal{F}'(x_i) = 0$, i.e., x_i is the extreme point of $\mathcal{F}(x)$, we obtain

$$c_i = x_i. \tag{51}$$

Based on the Assumption 1. (1), and (51), we get

$$b_i = \cos[2\pi(fx_i - \varphi)] \in \{-1, +1\}. \tag{52}$$

By means of the Taylor expansion at the point of x_i, the $u_i(x)$ and $\mathcal{F}(x)$ are given by

$$u_i(x) = u(x_i) + u'(x_i)(x - x_i) + \frac{u''(x_i)}{2!}(x - x_i)^2 + o\left[(x - x_i)^2\right], \tag{53}$$

and

$$\mathcal{F}(x) = \mathcal{F}(x_i) + \mathcal{F}'(x_i)(x - x_i) + \frac{\mathcal{F}''(x_i)}{2!}(x - x_i)^2 + o\left[(x - x_i)^2\right], \tag{54}$$

respectively. Based on the Assumption 1. (1), (2), (3), and (53), (54), we get

$$u''(x_i) \geq \mathcal{F}''(x_i), \tag{55}$$

i.e., $a_i \geq -2\pi^2 f^2 \cos[2\pi(fx_i - \varphi)]$. Due to $a_i \geq 0$, when $\cos[2\pi(fx_i + \varphi)] = 1$, we get $a_i = 0$, and when $\cos[2\pi(fx_i - \varphi)] = -1$, we get $a_i = 2\pi^2 f^2$. Therefore, a_i is given by

$$a_i = (1 - b_i)\pi^2 f^2. \tag{56}$$

If x_i satisfies $\mathcal{F}'(x_i) \neq 0$, we first consider the case $\mathcal{F}'(x_i) < 0$. $\mathcal{F}(x)$ can be rewritten as

$$\mathcal{F}(x) = \cos[2\pi f(x - \frac{\varphi}{f})]. \tag{57}$$

Fig. 17 illustrates the approximating of the objective function by an upper-bound quadratic function, when $\mathcal{F}'(x_i) < 0$. we observe that $c_i = p + n(T/2)$, where $p = \varphi/f$ is the phase, $T = 1/f$ is the cycle of $\mathcal{F}(x)$, and n is the nearest integer of half cycle towards $+\infty$. n satisfies

$$n = \left\lceil \frac{x - \varphi/f}{T/2} \right\rceil = \lceil 2(fx - \varphi) \rceil, \tag{58}$$

where $\lceil \cdot \rceil$ round the argument to the nearest integer towards $+\infty$. And thus, we get

$$c_i = \frac{\lceil 2(fx - \varphi) \rceil}{2f} + \frac{\varphi}{f}. \tag{59}$$

In a similar way, we get c_i when $\mathcal{F}'(x_i) > 0$

$$c_i = \frac{\lfloor 2(fx - \varphi) \rfloor}{2f} + \frac{\varphi}{f}. \tag{60}$$

where $\lfloor \cdot \rfloor$ round the argument to the nearest integer towards $-\infty$.

Based on the Assumption 1. (1), (2), and c_i, the parameters a_i and b_i are given by

$$a_i = \frac{-\pi f \sin[2\pi(fx_i - \varphi)]}{x_i - c_i}, \tag{61}$$

and

$$b_i = \cos[2\pi(fx_i - \varphi)] - a_i(x_i - c_i)^2, \tag{62}$$

respectively.

In summary, the parameters of the upper-bound quadratic function are given by
If x_i satisfies $\mathcal{F}'(x_i) = 0$,

$$\begin{cases} a_i = (1 - b_i)\pi^2 f^2, \\ b_i = \cos[2\pi(fx_i - \varphi)] \in \{-1, +1\}, \\ c_i = x_i, \end{cases} \tag{63}$$

Otherwise,

$$\begin{cases} a_i = \dfrac{-\pi f \sin[2\pi(fx_i - \varphi)]}{x_i - c}, \\ b_i = \cos[2\pi(fx_i - \varphi)] - a(x_i - c)^2, \\ c_i = \begin{cases} \dfrac{\lfloor 2(fx_i - \varphi) \rfloor}{2f} + \dfrac{\varphi}{f} & \text{if } F'(x_i) > 0, \\ \dfrac{\lceil 2(fx_i - \varphi) \rceil}{2f} + \dfrac{\varphi}{f} & \text{if } F'(x_i) < 0, \end{cases} \end{cases} \tag{64}$$

where $\lfloor \cdot \rfloor$ and $\lceil \cdot \rceil$ round the argument to the nearest integer towards $-\infty$ and $+\infty$, respectively.

REFERENCES

[1] X. Yu, Y. Fu, L. Nie, G. Zhao, and W. Zhang, "A waveform with low intercept probability for OFDM SAR," in *Proc. IEEE Prog. Electromagn. Res. Symp. (PIERS)*, Aug. 2016, pp. 2054–2058.
[2] L. Huang, K. Gao, Z. He, and J. Cai, "Cognitive MIMO frequency diverse array radar with high LPI performance," *Int. J. Antennas Propag.*, vol. 2016, May 2016, Art. no. 2623617.
[3] J. Li, H. Li, and S. Ouyang, "Identifying unambiguous frequency pattern for target localisation using frequency diverse array," *Electron. Lett.*, vol. 53, no. 19, pp. 1331–1333, Sep. 2017.
[4] A. Kalantari, M. Soltanalian, S. Maleki, S. Chatzinotas, and B. Ottersten, "Directional modulation via symbol-level precoding: A way to enhance security," *IEEE J. Sel. Topics Signal Process.*, vol. 10, no. 8, pp. 1478–1493, Dec. 2016.
[5] A.-M. Yao, P. Rocca, W. Wu, A. Massa, and D.-G. Fang, "Synthesis of time-modulated frequency diverse arrays for short-range multi-focusing," *IEEE J. Sel. Topics Signal Process.*, vol. 11, no. 2, pp. 282–294, Mar. 2017.
[6] C. Y. Mai, S. T. Lu, J. P. Sun, and G. H. Wang, "Beampattern optimization for frequency diverse array with sparse frequency waveforms," *IEEE Access*, vol. 5, pp. 17914–17926, 2017.
[7] T. Eker, S. Demir, and A. Hizal, "Exploitation of linear frequency modulated continuous waveform (LFMCW) for frequency diverse arrays," *IEEE Trans. Antennas Propag.*, vol. 61, no. 7, pp. 3546–3553, Jul. 2013.
[8] M. C. Wicks and P. Antonik, "Frequency diverse array with independent modulation of frequency, amplitude, and phase," U.S. Patent 7 319 427 B2, Jan. 15, 2008.
[9] H. Chen, H.-Z. Shao, and W. Q. Wang, "Joint sparsity-based range-angle-dependent beampattern synthesis for frequency diverse array," *IEEE Access*, vol. 5, pp. 15152–15161, 2017.
[10] S. Y. Nusenu, W.-Q. Wang, and S. Ji, "Secure directional modulation using frequency diverse array antenna," in *Proc. IEEE Radar Conf.*, May 2017, pp. 378–382.
[11] W.-Q. Wang, "Frequency diverse array antenna: New opportunities," *IEEE Antennas Propag. Mag.*, vol. 57, no. 2, pp. 145–152, Apr. 2015.
[12] J. Xiong, S. Y. Nusenu, and W.-Q. Wang, "Directional modulation using frequency diverse array for secure communications," *Wireless Pers. Commun.*, vol. 95, no. 3, pp. 2679–2689, Aug. 2017.
[13] J. Xiong, W.-Q. Wang, H. Shao, and H. Chen, "Frequency diverse array transmit beampattern optimization with genetic algorithm," *IEEE Antennas Wireless Propag. Lett.*, vol. 16, pp. 469–472, Jun. 2016, doi: 10.1109/LAWP.2016.2584078.
[14] K. Gao, W.-Q. Wang, J. Cai, and J. Xiong, "Decoupled frequency diverse array range–angle-dependent beampattern synthesis using non-linearly increasing frequency offsets," *IET Microw., Antennas Propag.*, vol. 10, no. 8, pp. 880–884, Mar. 2016.
[15] Y. Liu, H. Ruan, L. Wang, and A. Nehorai, "The random frequency diverse array: A new antenna structure for uncoupled direction-range indication in active sensing," *IEEE J. Sel. Topics Signal Process.*, vol. 11, no. 2, pp. 295–308, Mar. 2017.

[16] W. Khan, I. M. Qureshi, and S. Saeed, "Frequency diverse array radar with logarithmically increasing frequency offset," *IEEE Antennas Wireless Propag. Lett.*, vol. 14, pp. 499–502, 2015.
[17] W. Q. Wang and H. Z. Shao, "A flexible phased-MIMO array antenna with transmit beamforming," *Int. J. Antennas Propag.*, vol. 2012, Jan. 2012, Art. no. 609598.
[18] Y. Wang, W. Q. Wang, H. Chen, and H. Z. Shao, "Optimal frequency diverse subarray design with Cramér–Rao lower bound minimization," *IEEE Antennas Wireless Propag. Lett.*, vol. 14, pp. 1188–1191, 2015.
[19] W. Khan, I. M. Qureshi, A. Basit, M. Zubair, and S. U. Khan, "MIMO-frequency diverse array radar with unequal subarrays for improved range-angle dependent beamforming," *Wireless Pers. Commun.*, vol. 97, no. 2, pp. 1967–1984, Nov. 2017.
[20] F. Shu *et al.*, "Low-complexity and high-resolution DOA estimation for hybrid analog and digital massive MIMO receive array," *IEEE Trans. Commun.*, vol. 66, no. 6, pp. 2487–2501, Jun. 2018.
[21] Q. Cheng, J. Zhu, T. Xie, J. Luo, and Z. Xu, "Time-invariant angle-range dependent directional modulation based on time-modulated frequency diverse arrays," *IEEE Access*, vol. 5, pp. 26279–26290, 2017.
[22] Y. Ding, V. Fusco, and A. Chepala, "Circular directional modulation transmitter array," *IET Microw., Antennas Propag.*, vol. 11, no. 13, pp. 1909–1917, Oct. 2017.
[23] Z. Luo, H. Wang, and K. Zhou, "Polarization filtering based physical-layer secure transmission scheme for dual-polarized satellite communication," *IEEE Access*, vol. 5, pp. 24706–24715, 2017.
[24] X. Zhang, B. Zhang, and D. Guo, "Physical layer secure transmission based on fast dual polarization hopping in fixed satellite communication," *IEEE Access*, vol. 5, pp. 11782–11790, 2017.
[25] S. Yan, N. Yang, I. Land, R. Malaney, and J. Yuan, "Three artificial-noise-aided secure transmission schemes in wiretap channels," *IEEE Trans. Veh. Technol.*, vol. 67, no. 4, pp. 3669–3673, Apr. 2018.
[26] S. Wan *et al.*, "Power allocation strategy of maximizing secrecy rate for secure directional modulation networks," *IEEE Access*, vol. 6, pp. 38794–38801, 2018.
[27] F. Shu, L. Xu, J. Wang, W. Zhu, and Z. Xiaobo, "Artificial-noise-aided secure multicast precoding for directional modulation systems," *IEEE Trans. Veh. Technol.*, vol. 67, no. 7, pp. 6658–6662, Jul. 2018.
[28] F. Shu, X. Wu, J. Hu, J. Li, R. Chen, and J. Wang, "Secure and precise wireless transmission for random-subcarrier-selection-based directional modulation transmit antenna array," *IEEE J. Sel. Areas Commun.*, vol. 36, no. 4, pp. 890–903, Apr. 2018.
[29] T. Xie, J. Zhu, and Y. Li, "Artificial-noise-aided zero-forcing synthesis approach for secure multi-beam directional modulation," *IEEE Commun. Lett.*, vol. 22, no. 2, pp. 276–279, Feb. 2018.
[30] X. Zhang, X. Zhou, and M. R. McKay, "On the design of artificial-noise-aided secure multi-antenna transmission in slow fading channels," *IEEE Trans. Veh. Technol.*, vol. 62, no. 5, pp. 2170–2181, Jun. 2013.
[31] J. S. Hu, F. Shu, and J. Li, "Robust synthesis method for secure directional modulation with imperfect direction angle," *IEEE Commun. Lett.*, vol. 20, no. 6, pp. 1084–1087, Jun. 2016.
[32] J. Hu, S. Yan, F. Shu, J. Wang, J. Li, and Y. Zhang, "Artificial-noise-aided secure transmission with directional modulation based on random frequency diverse arrays," *IEEE Access*, vol. 5, pp. 1658–1667, 2017.
[33] J. Lin, Q. Li, J. Yang, H. Shao, and W.-Q. Wang, "Physical-layer security for proximal legitimate user and eavesdropper: A frequency diverse array beamforming approach," *IEEE Trans. Inf. Forensics Security*, vol. 13, no. 3, pp. 671–684, Mar. 2018.
[34] M. Razaviyayn, M. Hong, and Z.-Q. Luo, "A unified convergence analysis of block successive minimization methods for nonsmooth optimization," *SIAM J. Optim.*, vol. 23, no. 2, pp. 1126–1153, 2013.
[35] S. Goel and R. Negi, "Guaranteeing secrecy using artificial noise," *IEEE Trans. Wireless Commun.*, vol. 7, no. 6, pp. 2180–2189, Jun. 2008.
[36] F. Shu, X. Wu, J. Li, R. Chen, and B. Vucetic, "Robust synthesis scheme for secure multi-beam directional modulation in broadcasting systems," *IEEE Access*, vol. 4, pp. 6614–6623, 2016.

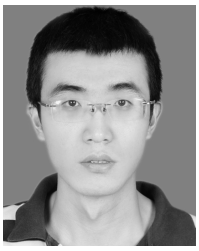

BIN QIU received the B.S. degree from the School of Mathematics and Computing Science, Changsha University of Science and Technology, Changsha, China, in 2012, and the M.S. degree from the School of Electronic Engineering, Xi'an Shiyou University, Xi'an, China, in 2015. He is currently pursuing the Ph.D. degree with the Department of Information and Communications Engineering, Northwestern Polytechnical University, Xi'an. His research interests include wireless communications, array signal processing, and physical-layer security.

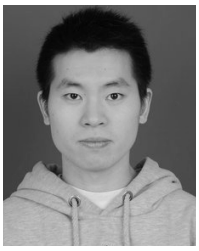

JIAN XIE received the M.Sc. and Ph.D. degrees from the School of Electronic Engineering, Xidian University, in 2012 and 2015, respectively. He is currently an Assistant Professor with Northwestern Polytechnical University. His research interests include antenna array processing and radar signal processing.

LING WANG received the B.Sc., M.Sc., and Ph.D. degrees from Xidian University, Xi'an, China, in 1999, 2002, and 2004, respectively, all in electronic engineering. From 2004 to 2007, he was at Siemens and Nokia Siemens Networks. Since 2007, he has been with the School of Electronic and Information, Northwestern Polytechnical University, Xi'an, and was promoted to Professor in 2012. His current research interests include array processing and smart antennas, wideband communications, cognitive radio, adaptive antijamming for satellite communications, satellite navigation, and date link systems.

YUEXIAN WANG received the B.S. degree in electronics and information engineering from Northwestern Polytechnical University, China, in 2006, the M.Eng.S. and Ph.D. degrees in electrical and electronic engineering from The University of Adelaide, Australia, in 2012 and 2015, respectively. From 2015 to 2017, he was a Post-Doctoral Fellow at The University of Adelaide. Since 2018, he has been with the School of Electronics and Information, Northwestern Polytechnical University. His current research interests include array signal processing, compressed sensing, tensor decomposition, and their applications to radar, sonar, and wireless communications.